Landes Bioscience www.landesbioscience.com

Supplemental Material to:

Cindy Meyer, Katharina Berg, Katja Eydeler-Haeder, Inken Lorenzn, Joachim Grötzinger, Stefan Rose-John, Ulrich Hahn

Stabilized Interleukin-6 receptor binding RNA aptamers

2013; 11(1)
http://dx.doi.org/10.4161/rna.27447

www.landesbioscience.com/journals/rnabiology/article/27447/

Supplementary data for

Single-molecule FRET supports the two-state model of Argonaute action

Adrian Zander, Phil Holzmeister, Daniel Klose, Philip Tinnefeld and Dina Grohmann

Inventory of Supplementary Data

1 Purification of recombinant *M.jannaschii* Argonaute

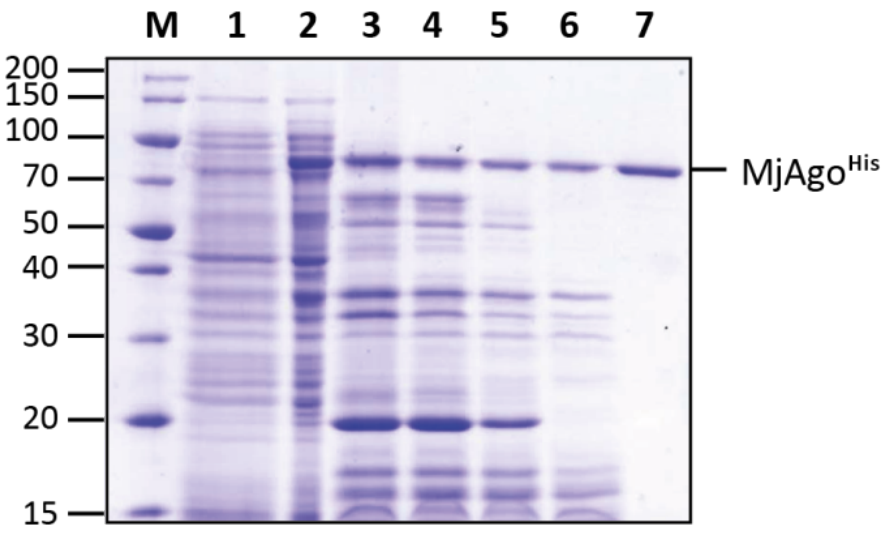

Figure S1: Purification of *M.jannaschii* Ago. Protein expression and purification was analysed by SDS-PAGE (12%). The gel was stained with Coomassie Brilliant Blue. The position of MjAgo (theoretical molecular weight: 84.5 kDa) is indicated. The molecular weight of a protein standard is loaded in lane M and sizes are indicated. Lane 1: bacterial extract of E.coli/Rosetta cells without recombinant protein synthesis; lane 2: bacterial extract of E.coli/Rosetta cells after addition of a final concentration of 1 mM IPTG and expression of MjAgo for 3 hours; lane 3: total bacterial extract; lane 4/5/6: supernatant after heat inactivation for 15 min of the bacterial extract at 65°C, 75°C and 85°C, respectively; lane 7: purified MjAgo after Ni-NTA purification.

2 Sequence alignment *M.jannaschii* Ago and *P.furiosus* Ago

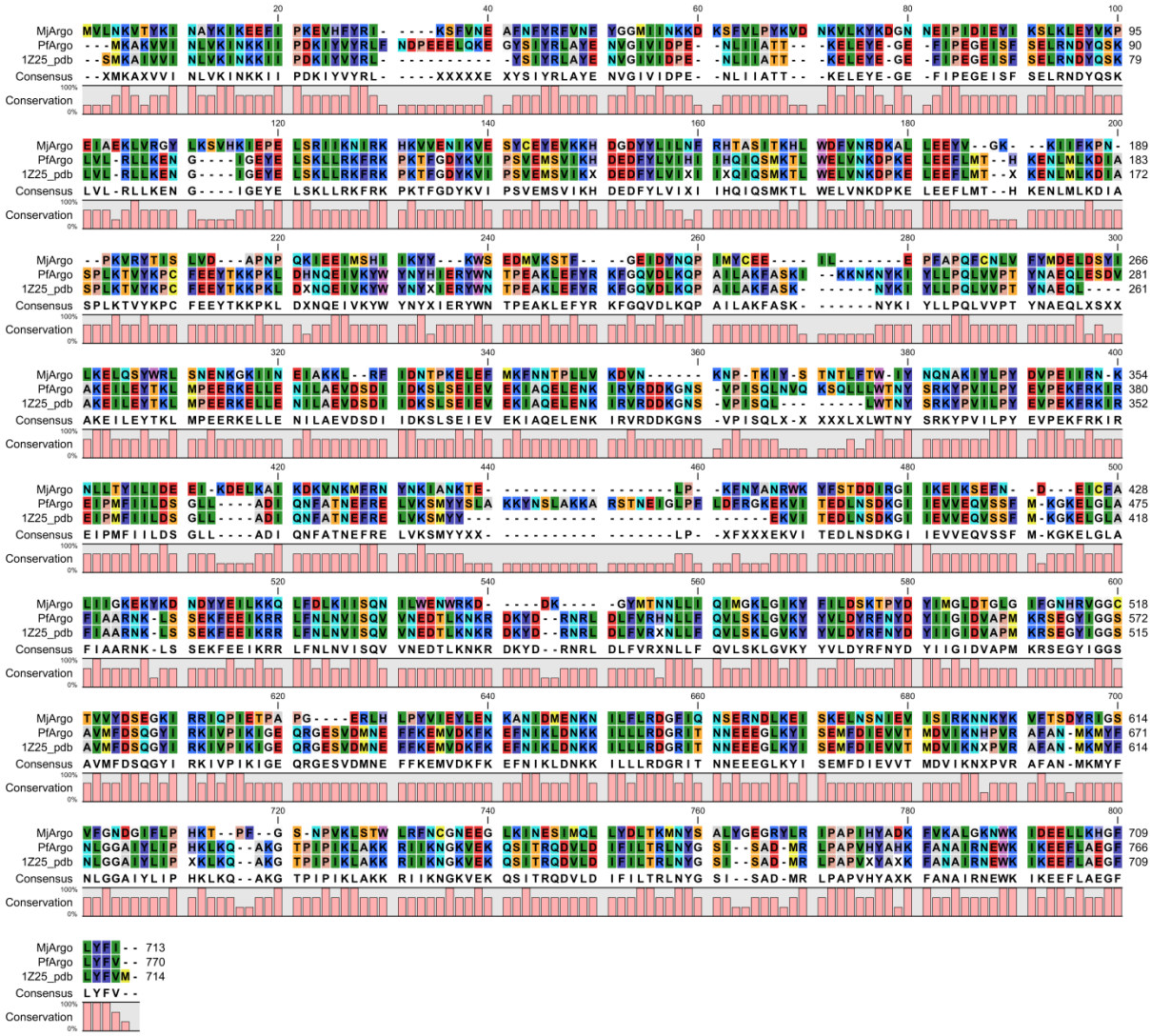

Figure S2: Amino acid sequence alignment of Ago proteins from *M.jannaschii* and *P.furiosius* (full sequence and crystallized part, PDB: 1Z25) that we used as template for the homology model. The alignment has been created using the CLC Sequence Viewer 6.3 software (www.clcbio.com).

3 Structural alignment of *M.jannaschii* Ago and *H.sapiens* Ago2

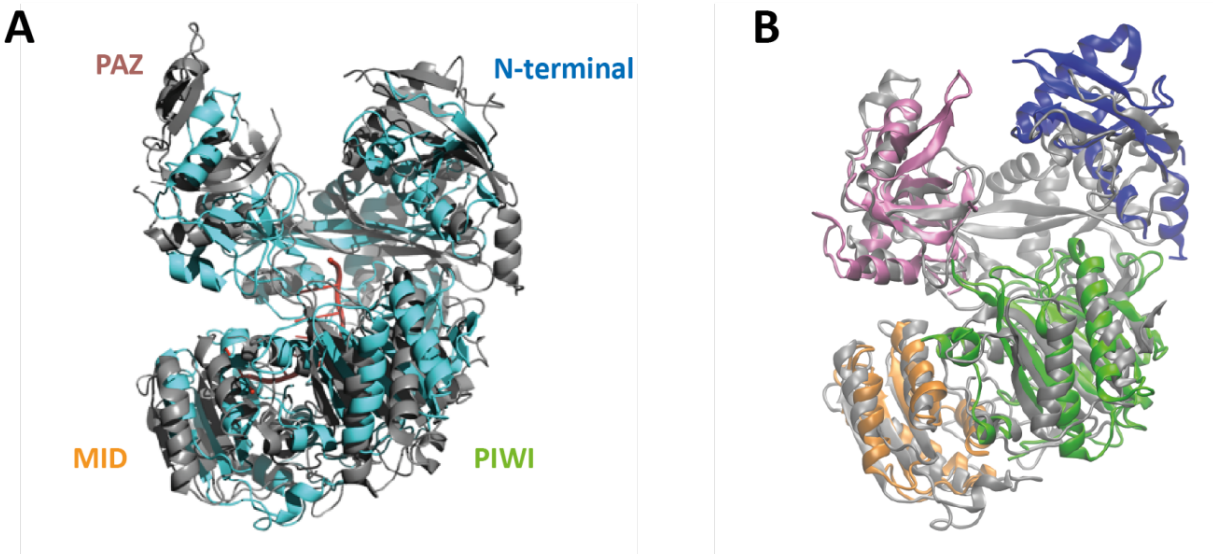

Figure S3: Structural alignment of the *M.jannaschii* Ago model with the structure of *H. sapiens* Ago2. A. Overall structural alignment of MjAgo (coloured in cyan) with the structure of the HsAgo2 (grey, PDB: 4EI3)**.** The RNA bound to the *H. sapiens* Ago is highlighted in red. The proteins are orientated as shown in Figure 1 and the relative domain orientation is indicated by the domain abbreviations. **B.** Alignment of the individual domains of HsAgo2 with the MjAgo homology structure. MjAgo is shown in grey and the individual domains of HsAgo are coloured (PAZ domain in pink, the MID domain in orange, the PIWI domain in green and the N-terminal domain in blue).

4 Interaction of labelled guide strand DNA with MjAgo

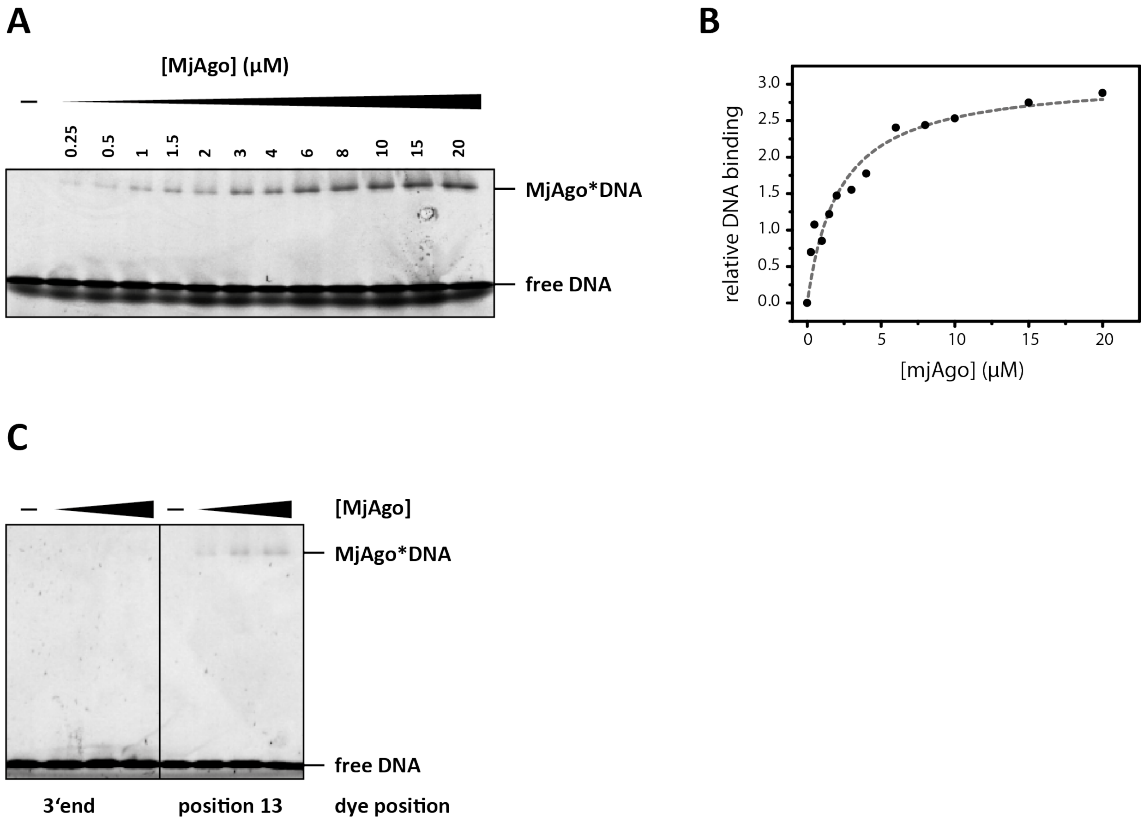

Figure S4: Interaction of the DNA guide strand with *M.jannaschii* Ago. A. EMSA showing the complex formation between MjAgo and the DNA guide strand (333 nM) labelled with the fluorescent dye Atto550 at position 18. **B.** Quantification of the bound DNA fraction allows direct fitting of the titration curve yielding a dissociation constant of 2.2 (±0.4) µM. **C.** EMSA showing the complex formation between MjAgo (0, 1, 3, 5 µM) and guide strands (333 nM) that carry the Atto550 dye at nucleotide 13 or the 3'end.

5 Influence of dye chemistry and His-tag on DNA binding efficiency

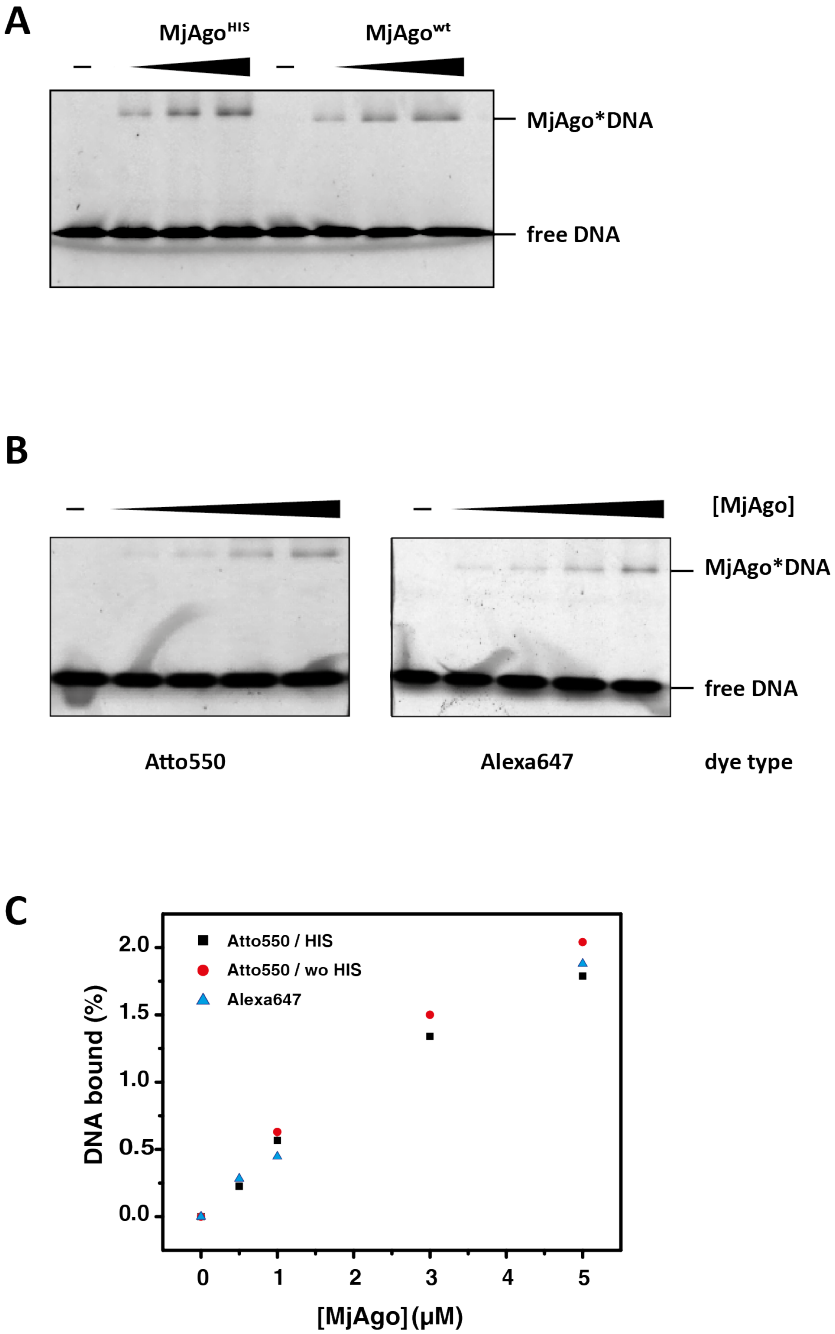

Figure S5: The His_6-Tag and the dye type do not influence the binding efficiency of the guide strand. **A**. EMSA of MjAgo-guide DNA complexes using guide DNA labelled with Atto550 at position 13 (333 nM) and increasing concentrations of MjAgo (0, 1, 3, 5 µM). **B**. EMSA of MjAgo-guide DNA complexes using guide DNA labeled with Atto550 or Alexa647 at position 13 (333 nM) and increasing concentrations of MjAgo (0, 0.5, 1, 3 5 µM). **C**. Quantification of the amount of DNA bound for the different DNA oligonucleotides and MjAgo variants shown in (A) and (b) relative to the total amount of labelled DNA signal in the complete lane.

6 Establishment of cleavage conditions for *M.jannaschii* Ago

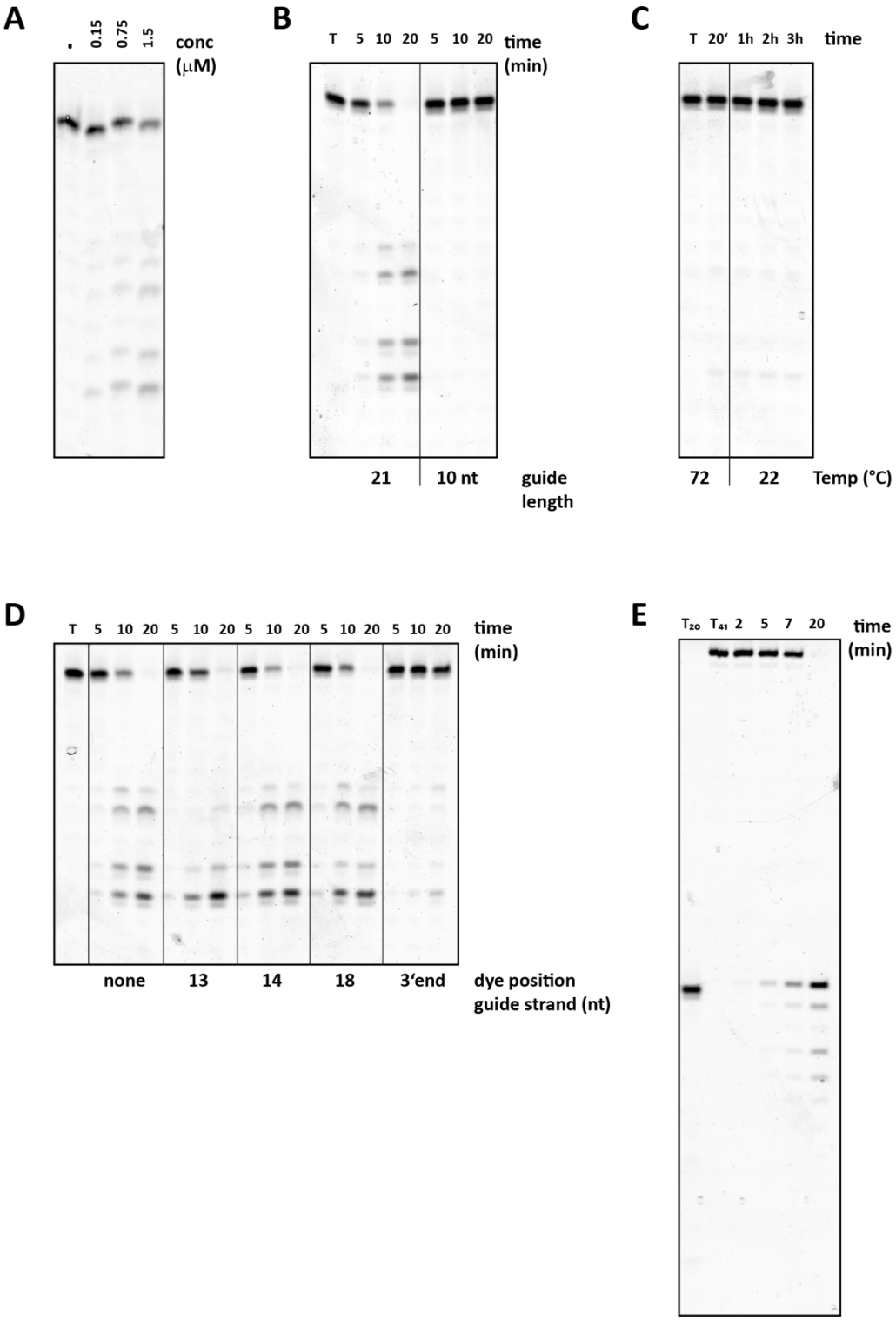

Figure S6: Establishment of cleavage conditions using DNA-guide-loaded *M.jannaschii* Argonaute. If not indicated otherwise the cleavage reactions were carried out using 0.6 µM MjAgo, 1.7 µM guide and 0.72 µM target strand at 85°C. Reactions were stopped at the indicated time points. The lane labelled with "T" refers to a control reaction in the absence of MjAgo carried out under identical conditions. The cleavage products were resolved on a

12% denaturing polyacrylamide gel. **A.** The cleavage reaction is concentration-dependent as the intensity of the cleavage products intensifies while the substrate band is reduced with increasing MjAgo concentrations (0.15, 0.75, 1.5 μM). The reactions were stopped after 10 min. **B.** Cleavage does not occur if the DNA guide strand is 10 nt in length as compared to the standard guide strand with 21 nt. **C.** Cleavage does not occur under reaction conditions chosen for complex formation in preparation of the single-molecules experiments. The labelled MjAgo and DNA are incubated for 20 min at 72°C first to promote complex formation (time point 20 min in the panel). Subsequently, the complex is purified via gel filtration (1h at room temperature, time point 1h in the panel) and the single molecule data were recorded for another 2 hours at 22°C (time points 2h and 3h at 22°C).
D. Cleavage is strongly reduced if a DNA guide strand with an Atto550-label at the 3'end is used. **E.** MjAgo efficiently utilizes a long DNA target (41 nt in length, T_{41}) that contains a sequence motive complementary to the let-7 guide DNA (see table S1 for full sequences). T_{20} refers to the standard target 20 nt in length that is loaded for comparison.

7 Structural information about the position of the labelling positions in the DNA guide strand

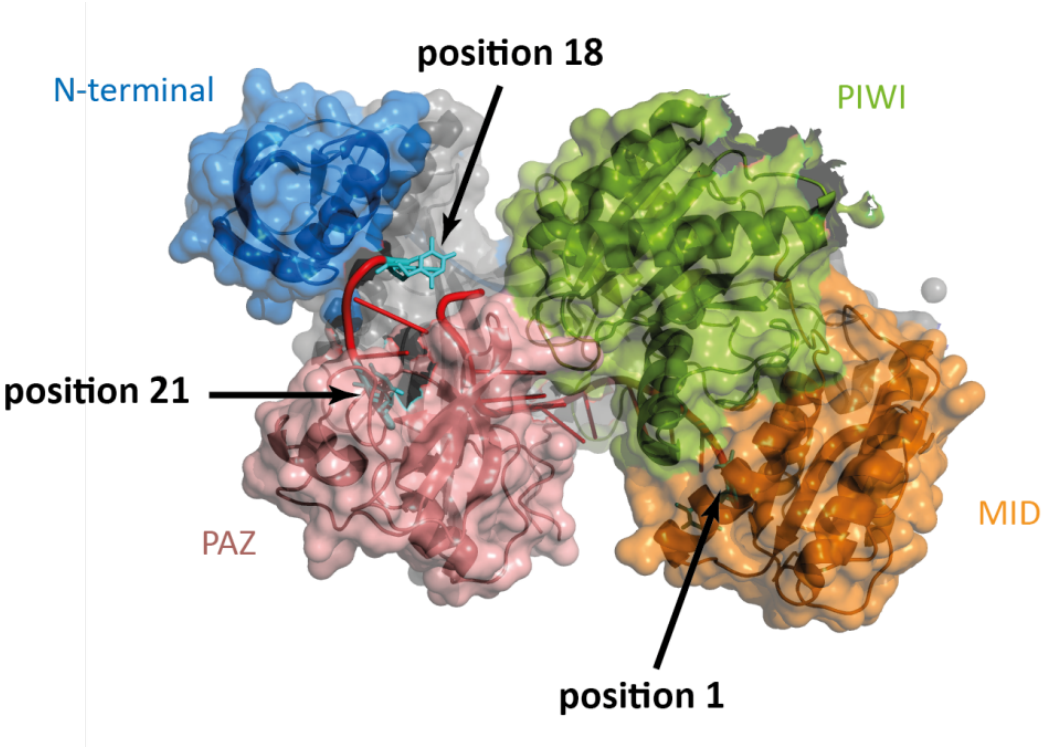

Figure S7: Positioning of nucleotide 1 (5' end), 18 and 21 (3' end) of the DNA guide. Path of the guide DNA bound to *T. thermophilus* Ago (PDB: 3DLH). The N-terminal domain is shown in blue, the PAZ domain in salmon, the MID domain in orange, the PIWI domain in green and the DNA guide strand in red. The path of the DNA is traceable for nucleotides 1-11 and 18-21.Nucleotides 1, 18 and 21 are highlighted in cyan. The 3' end of the DNA is bound in the PAZ domain whereas the 5' is buried in a binding pocket located in the MID domain. Unlike position 1 and 21 the base at position 18 is not involved in interactions with the protein.

8 DNA-binding activity and site-specific labelling of *M.jannaschii* Ago mutants via Staudinger Ligation

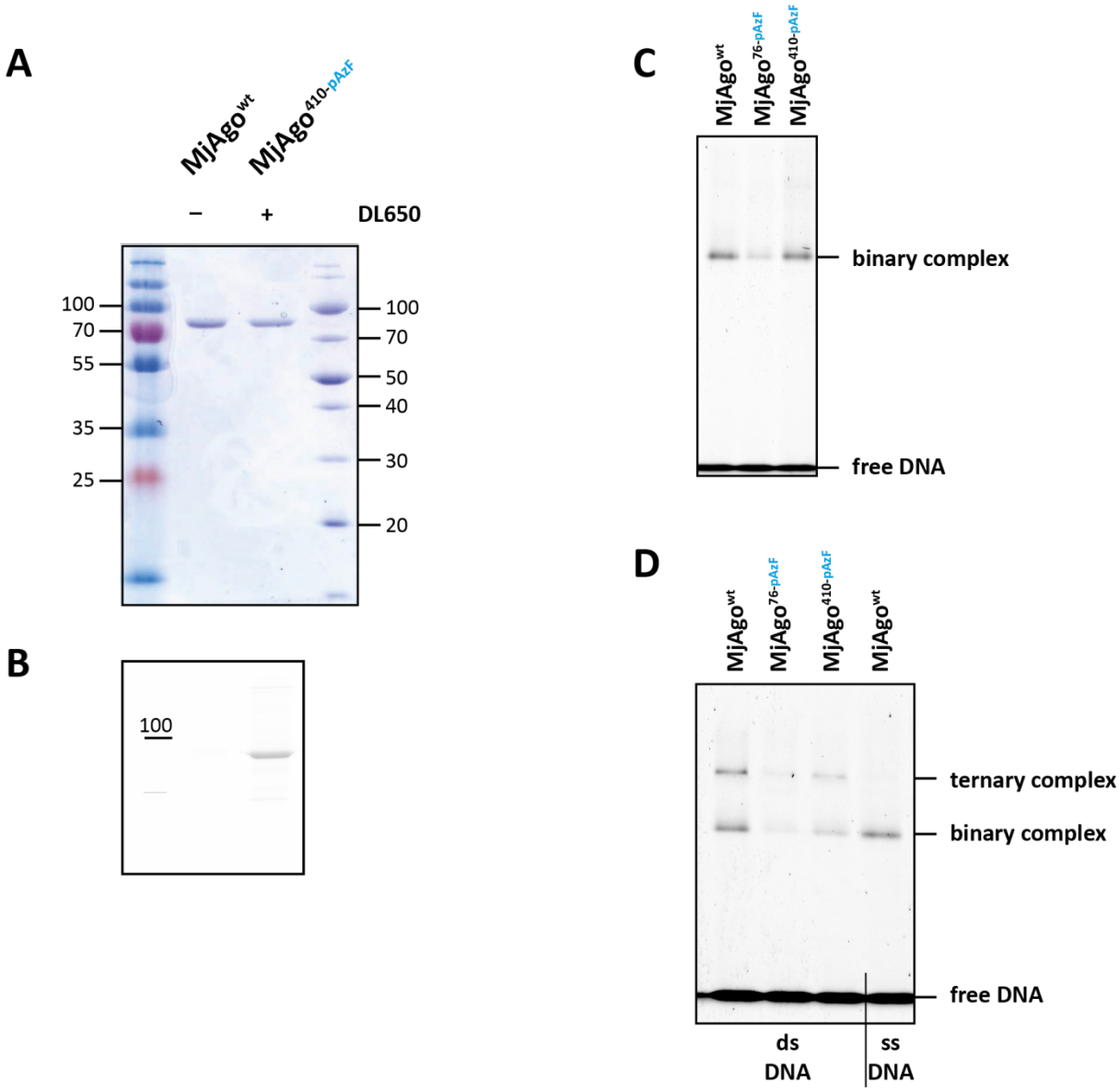

Figure S8: Production and activity control of site-specifically labeled archaeal Ago variants. **A**. Full length MjAgo carrying the unnatural amino acid p-Azidophenylalanine (AzF) is purified using a genetically encoded His6-tag at the C-terminus of the protein. Shown is the MjAgo^{I410Azf} mutant. **B**. Fluorescence scan of the SDS-PAGE gel shown in (A) detecting the fluorescence of the DyLight650 dye (excitation: 635 nm, emission: 670 nm). Addition of the fluorescent probe DyLight650 that carries a phosphine group specifically couples the dye to the azide moiety of AzF via the Staudinger-Bertozzi ligation but not to the wt protein. **C** and **D**. The mutated MjAgo^{N76AzF} and MjAgo^{I410AzF} variants are able to specifically and efficiently bind the guide strand and the guide/target strand duplex (both labelled with Atto550 at

position 18 in the guide strand) in a manner comparable to the wt MjAgo protein (2.8 µM). The MjAgo^{S221AzF} mutant could not be included as the yields of this mutant were not high enough to reach concentrations necessary to visualize DNA binding on the ensemble level.

9 E-S Histograms of the single-molecule FRET measurements

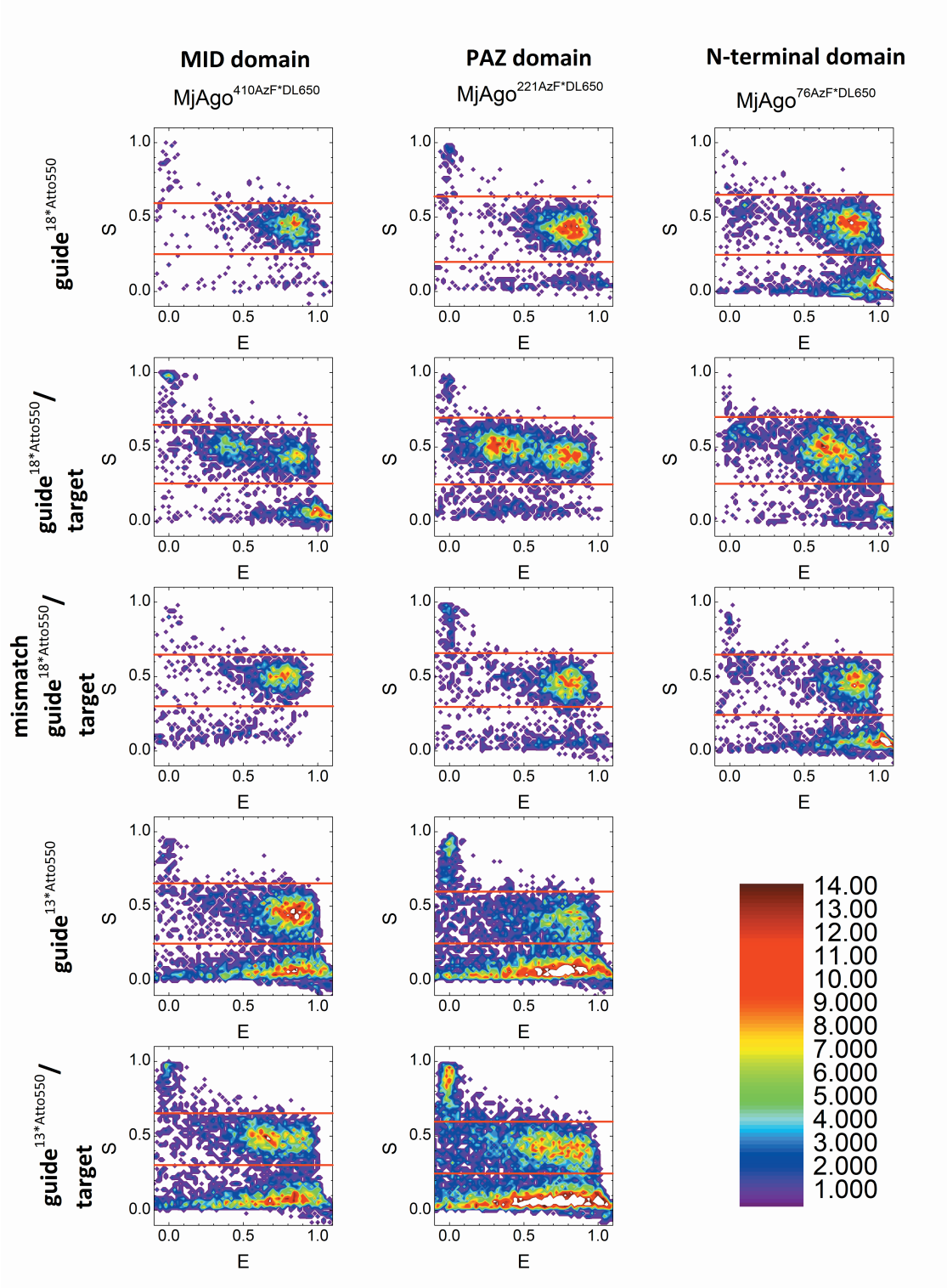

Figure S9: **E-S histograms for dual-labeled binary and ternary MjAgo complexes.** We calculate the proximity ratio E and the stoichiometry S for each detected molecule and generate two-dimensional histograms for all combinations of labeled MjAgo complexes in order to separate the different populations [1]. Molecules with an S value close to 1 represent donor only species (DNA guide strand only) while an S value close to 0 represents the

acceptor only species (uncoupled DyLight650 only/or unliganded labelled MjAgo). Molecules with a medial S value appear only when an acceptor and a donor dye diffuse through the focus at the same time and represent the Ago-nucleic acid complexes. The majority of donor-only and acceptor-only labelled molecules as well as bursts arising from coincidental co-localisation of donor and acceptor molecules have been removed from the E-S histogram using recently developed filters [2] that check for stability of the fluorescence signal within the individual fluorescent bursts. The FRET populations are selected (area between red lines) and presented as one-dimensional histograms in Fig.5 and Fig.6 of the main text. Correction factors, filter settings and selection values can be found in Table S3 in the Supplementary Methods section.

10 Conformational changes in *the T.thermophilus* Ago protein

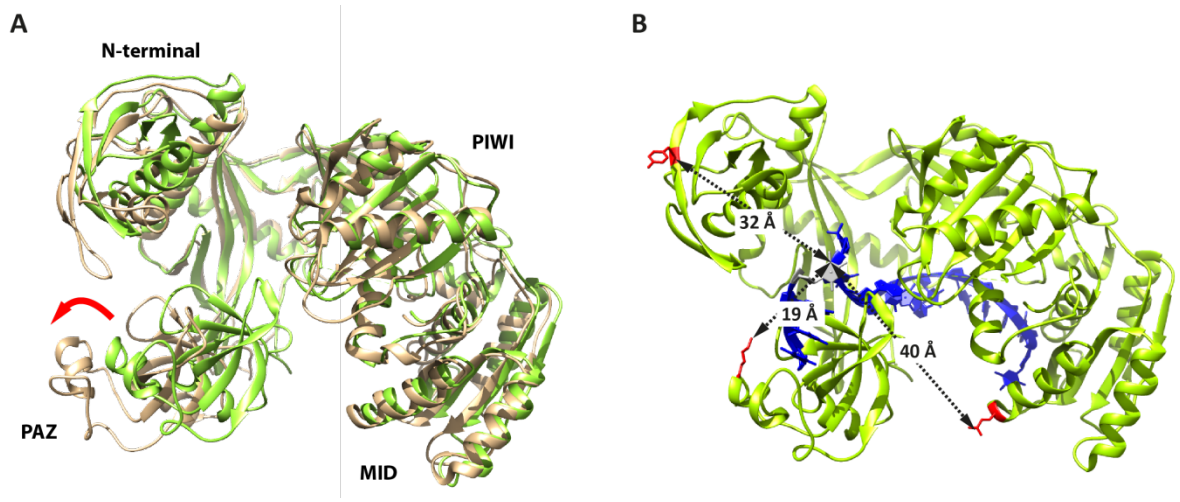

Figure S10: Conformational changes in the *T. thermophilus* Ago protein upon nucleic acid binding. A. Structural alignment of the binary complex with bound guide DNA (PDB: 3DLH, green) with the tertiary complex with bound guide-target DNA duplex (PDB: 3HK2, beige). The nucleic acids are removed for clarity. The structures are orientated with respect to their PIWI domain and domain names are assigned. The red arrow indicates the conformational change of the PAZ domain upon binding of the guide-target duplex. **B.** TtAgo in complex with the guide DNA (PDB: 3DLH) showing the distances between nucleotide 18 in the guide strand (highlighted in grey) and the amino acids (T91, Lys230, Glu 416) corresponding to the labelled positions in MjAgo (highlighted in red).

11 **Sub-millisecond dynamics of Ago-DNA complexes**

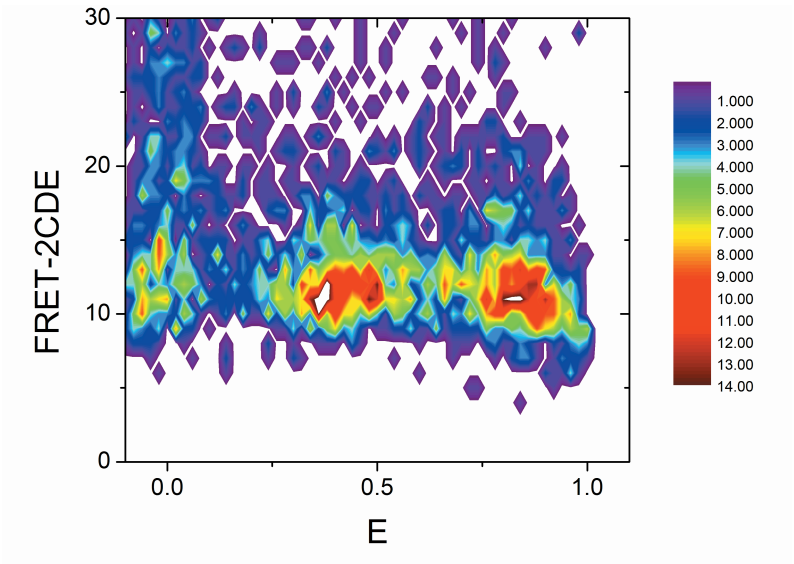

Figure S11: **No fluctuations of the FRET efficiency faster than the diffusion time.** Two-dimensional histogram of the FRET-2CDE value and the FRET efficiency E for the dsDNA (Donor position in the guide strand position 18) measurement (S-values 0.25-0.65, no ALEX-2CDE filter). The FRET-2CDE value reports on fluctuations of the FRET-efficiency within each burst. Hence, dynamics faster than the diffusion time would result in an E-value between the two main populations and an increased FRET-2CDE value (compare [2]), which is not observed here. Therefore, our data rule out dynamics between the two detected FRET populations on timescales shorter than the diffusion time.

12 **Table S1: Nucleic acid substrates used in this study.**

Name	Sequence	Dye	Position of the label
guide DNA_3'	5' p-TGAGGTAGTAGGTTGTATAGT	Atto550	3' end
guide DNA_13	5' p-TGAGGTAGTAGGTTGTATAGT	Atto550	Attached to T at position 13
guide DNA_14	5' p-TGAGGTAGTAGGTTGTATAGT	Atto550	Attached to T at position 14
guide DNA_14_647	5' p-TGAGGTAGTAGGTTGTATAGT	Alexa647	Attached to T at position 14
guide DNA_18	5' p-TGAGGTAGTAGGTTGTATAGT	Atto550	Attached to T at position 18
guide DNA_10 nt	5' p-TGAGGTAGTA	-	
guide RNA	5' p-UGAGGUAGUAGGUUGUATAGU	-	
guide RNA_18	5' p-UGAGGUAGUAGGUUGUATAGU	Atto550	Attached to T at position 18
target DNA	5' - TATACAACCTACTACCTCGT	-	
target DNA_AF647	5' - TATACAACCTACTACCTCGT	Alexa647	Attached to T at position 17
target DNA_bubble	5' - TATACAACtcACTACCTCGT	Alexa647	Attached to T at position 17
target DNA_long	5' – AGGTGATAAGACTATACAACCTA CTACCTCGTAATGTCCGT	Alexa647	Attached to 5' end
target RNA	5' - UAUACAACCUACUACCUCGU	-	
target RNA_TAMRA	5' - UAUACAACCUACUACCTCGU	TAMRA	Attached to T at position 17

13 Supplementary Methods

13.1 Loop refinement.

To relax insertions which are neither sufficiently restrained nor sampled well in the previous approach, loop refinement in Modeller [3] was applied in subsequent steps to 9 insertions generating 50 models at each step followed by selection of the best model in terms of its DOPE score. Hereafter, one loop region, residues 389 to 398 still indicated insufficient sampling by its stereochemistry and was subjected to repeated simulated annealing minimization in Yasara using its NOVA force field. [4] The scores and stereochemistry assessed with PROCHECK [5] of the final model and the template structure are summarized in Tab. 1.

13.2 Table S2: Modelling scores and stereochemistry of the best model and template structure.

	Model	Template	comment
normalized DOPE score	-0.792	-1.385	lower=better (about -1 is native-like)
DOPE score	-87118.4	-93777.2	lower=better, not normalized
GA-341 score	1.0	1.0	0 to 1(best) for fold assessment
TM score [6]	0.91900	---	
equiv. Ca RMSD	1.45 (over 666 Cas)	---	
Sequence Identity	27.171 %	---	
Ramachandran: good	82.6 %	83.7 %	
allowed	15.8 %	15.3 %	
generous	1.4 %	0.9 %	
disallowed	0.2 %	0 %	

13.3 Table S3: Correction factors, filter settings and selection criteria for single-molecule data in Fig. S10.

complex	dx	lk	ALEX-2CDE	FRET-2CDE		S	
			max	**min**	**max**	**min**	**max**
MjAgo^{l410Azf}+guide^{18}	0.048	0.139	12	8	12	0.25	0.60
MjAgo^{l410Azf} +guide^{18}/target	0.059	0.123	12	5	15	0.25	0.65
MjAgo^{l410Azf} + mismatch guide^{18}/target	0.050	0.150	9	8	12	0.30	0.65
MjAgo^{l410Azf}+guide^{13}	0.059	0.172	10	8	12	0.25	0.65
MjAgo^{l410Azf} +guide^{13}/target	0.063	0.177	10	8	12	0.30	0.65
MjAgo^{S221Azf} +guide^{18}	0.057	0.130	11	7	13	0.20	0.65
MjAgo^{S221Azf} +guide^{18}/target	0.062	0.144	9	8	12	0.25	0.70
MjAgo^{S221Azf} + mismatch guide^{18}/target	0.060	0.147	12	7	13	0.25	0.65
MjAgo^{S221Azf} +guide^{13}	0.058	0.159	10	8	12	0.25	0.60
MjAgo^{S221Azf} +guide^{13}/target	0.062	0.150	10	7	13	0.25	0.60
MjAgo^{N76Azf} +guide^{18}	0.060	0.142	10	7	13	0.25	0.65
MjAgo^{N76Azf} +guide^{18}/target	0.059	0.143	10	7	13	0.25	0.70
MjAgo^{N76Azf} + mismatch guide^{18}/target	0.062	0.147	9	8	12	0.25	0.65

Supplementary References

1 Kapanidis, A. N. *et al.* Fluorescence-aided molecule sorting: analysis of structure and interactions by alternating-laser excitation of single molecules. *Proc Natl Acad Sci U S A* **101**, 8936-8941, doi:10.1073/pnas.0401690101 (2004).

2 Tomov, T. E. *et al.* Disentangling subpopulations in single-molecule FRET and ALEX experiments with photon distribution analysis. *Biophysical journal* **102**, 1163-1173, doi:10.1016/j.bpj.2011.11.4025 (2012).

3 Fiser, A., Do, R. K. & Sali, A. Modeling of loops in protein structures. *Protein Sci* **9**, 1753-1773, doi:10.1110/ps.9.9.1753 (2000).

4 Krieger, E., Koraimann, G. & Vriend, G. Increasing the precision of comparative models with YASARA NOVA--a self-parameterizing force field. *Proteins* **47**, 393-402 (2002).

5 Laskowski, R. A. M., M. W.; Moss, D. S.; Thornton, J. M. . PROCHECK: a program to check the stereochemical quality of protein structures. *Journal of Applied Crystallography* **26**, 283 - 291 (1993).

6 Zhang, Y. & Skolnick, J. Scoring function for automated assessment of protein structure template quality. *Proteins* **57**, 702-710, doi:10.1002/prot.20264 (2004).